JOURNAL OF MATERIALS SCIENCE 27 (1992) 5426–5434

Influence of carbon content on microstructure and tempering behaviour of $2\frac{1}{4}$ Cr 1 Mo steel

P. PARAMESWARAN, M. VIJAYALAKSHMI, P. SHANKAR, V. S. RAGHUNATHAN
Physical Metallurgy Section, Indira Gandhi Centre for Atomic Research, Kalpakkam-603 102, India

Transmission electron microscopic studies aimed at elucidating the effect of carbon level on the tempering behaviour of $2\frac{1}{4}$ Cr 1 Mo steels have been carried out. Specimens with two different carbon levels (0.06% and 0.11%) were cooled in flowing argon gas (AC) from an austenitization temperature of 1323 K and tempered at 823, 923 and 1023 K for times ranging from 2 to 50 h. The tempering behaviour at these temperatures for the two carbon levels is found to differ in the nature of secondary hardening at lower temperatures, variation in the time to peak hardness and the saturation level of hardness at long tempering times. Based on a detailed study, using analytical electron microscopy, on the morphology, crystallography and microchemistry of secondary phases, the factors governing the observed variations in tempering behaviour are related to the difference in the dissolution rate of bainite, nucleation of acicular M_2C carbides and transformation rate of primary carbides into secondary alloy carbides. The carbides which promote softening were identified as M_7C_3, $M_{23}C_6$ and M_6C, whereas hardening is mainly imparted by M_2C.

1. Introduction

The low alloy $2\frac{1}{4}$ Cr 1 Mo steel has been widely used in steam generator piping for nuclear power plants, especially the sodium-cooled fast reactors [1–4]. Considerable effort has been made to understand the metallurgical factors that influence high temperature properties, as is clear from the enormous wealth of published information available on these steels.

Almost all the literature available on $2\frac{1}{4}$ Cr 1 Mo steels emphasizes only those features which confer long-term creep resistance to these steels. Of these studies, many are confined mostly to 0.1% carbon steel, in either normalized and tempered or annealed state, since it finds its widest application in one of these conditions. Even the oft-quoted carbide stability diagrams [5] evaluated by Baker and Nutting are confined to 0.1% carbon steel, in the quenched and normalized conditions. Although they provide very valuable information, the phase fields of different carbides are reported to be extremely sensitive to minor alloying additions. Therefore, it is considered prudent to establish these diagrams for various alloys and as a result, the precipitation of carbides has been the subject of several investigations [5–10].

The sequence of carbide precipitation evaluated above assumes relevance in the context of embrittlement behaviour of $2\frac{1}{4}$ Cr 1 Mo steels. Particularly, it has been predicted [11, 12] that increase in dissolved Mo and decrease in dissolved Cr enhance segregation of P to the grain boundary. It has been found that segregation of P to the grain boundary is enhanced by Mn and Si. Based on these studies, an empirical correlation between activity of various minor elements and degree of embrittlement has been arrived at [12], and is expressed as $J = 10^4\ \{([Mn] + [Si]) \times ([P] + [Sn])\}$. The existence of such a correlation obviously stems from the fact that changes in matrix composition consequent to carbide transformation play a crucial role in the segregation process. Of late, attempts even to predict and assess the residual life of a component based on characterization of changes in morphology and composition of carbides are in progress [13]. Additionally, the existence of carburization and decarburization due to mass transfer between structural materials of the steam generator and intermediate heat exchanger in liquid metal fast-breeder reactors, has imposed the need for studying the effect of carbon content on the behaviour of these steels [14]. These studies offer an insight – at least qualitatively – into how the loss of carbon would modify the microstructure and hence the mechanical properties.

The object of the present work is to understand the effect of carbon level on the tempering behaviour of $2\frac{1}{4}$ Cr 1 Mo steel and the micromechanisms responsible for the observed differences when the steel is tempered over a range of temperatures. Since the ASME pressure vessel code case 1331.8 recommends a material of minimum 0.07 wt % C to a maximum of 0.15 wt % C, the experimental work was planned on materials of these extreme carbon levels in the tempering range 823–1023 K.

2. Experimental procedure

All the experiments were conducted on specimens cut from 10 mm diameter bars and 6 mm square rods

0022–2461

whose chemical compositions are given in Table 1. The specimens of carbon level 0.06% and 0.11% will be hereafter referred to as steel A and steel B, respectively.

Specimens were austenitized at 1323 K for 1 h in a vacuum of 1.333×10^{-3} pascal in a vacuum furnace. They were subsequently cooled by Ar purging in the furnace. Tempering of the specimens was carried out at 823, 923 and 1023 K for various times ranging from 2 to 50 h. Macrohardness tests were performed on all the tempered specimens using a Vickers macrohardness tester (load = 1 kg).

Optical microscopy was carried out by standard metallographic procedures of preparation. Thin foils for electron microscopy were prepared by jet thinning of 0.15 mm sheets using a 10% perchloric acid and 90% acetic acid electrolyte which were observed in a Philips EM 400T microscope. Carbon replicas of etched surfaces were prepared and used for carrying out analytical electron microscopic studies of the carbides in a Philips EM 430 microscope.

3. Results

Fig. 1 shows the variation of macrohardness in both steels as a function of time for various tempering temperatures, namely 823, 923 and 1023 K. Steel B exhibited higher Vickers Hardness than steel A in argon-cooled (AC) condition. Generally, the tempering behaviour of the steels remained the same except for the presence of secondary hardening peaks at the lower temperatures of 823 and 923 K but not at 1023 K. At a given temperature, the hardness reached maximum much faster in steel B than in steel A. At 1023 K, both the steels exhibited marked softening compared with the moderate softening rate at lower temperatures. Correspondingly, the saturation value after prolonged tempering at 1023 K is much lower than the corresponding values at 823 and 923 K.

Similar trends in the tempering behaviour have been reported in many earlier studies on $2\frac{1}{4}$ Cr 1 Mo steels. Baker and Nutting [5] observed only very slight increase in the hardness at 673 K and 823 K for the water-quenched steels, which has been attributed to conversion of ε carbide to cementite and precipitation of acicular Mo_2C carbides, respectively. Leitnaker *et al.* [10] have reported only continuous softening without any secondary hardening, probably due to the high temperature of tempering. The initial treatment prior to tempering in most of the earlier studies is either water quenching or normalizing. The deliberate choice of very low cooling rate in the present study has enabled maximization of the extent of secondary hardening (Fig. 1), which is much more prominent than that reported previously.

The optical micrographs of both the steels in AC condition (Fig. 2a and b) illustrate that the steels develop a mixture of polygonal ferrite and granular bainite. The volume fraction of bainite was found to be higher in steel B (30%) than in steel A (18%). The ferrite grains were free of any optically resolvable carbides. Optical microscopy studies of tempered steels suggest that the dissolution rate of bainite depends on both carbon content and tempering temperatures. Fig. 3 shows a set of optical micrographs illustrating the dependence of dissolution rate of bainite on carbon content and tempering temperature. The dissolution of bainite was found to be complete at 1023 K within 2 h for steel A (Fig. 3a) and 8 h for steel B whereas bainite was found to be present despite prolonged tempering times of 50 h at 923 K and 823 K for both steels (Fig. 3c to f). Tempering at 1023 K for 2 h had resulted in complete dissolution of bainite in steel A (Fig. 3a) in contrast to retention of a small fraction of bainite in steel B (Fig. 3b). This observation suggests that reduction in carbon level accelerates dissolution of bainite. The salient features of these studies are as follows:

(a) The amount of bainite in the argon-cooled steels is greater for steel B (30%) than steel A (18%).
(b) Reduction in the carbon content of the steel favoured the dissolution of bainite.
(c) The dissolution of bainite was rapid and complete for both steels at 1023 K and incomplete at 923 K and 823 K up to 50 h.

Transmission electron microscopy studies of thin foils of steel A and steel B revealed several interesting features.

TABLE I Chemical composition of steels A and B used in the present study

Alloy	C	Si	Mn	P	Cr	Mo
Steel A	0.060	0.19	0.48	0.007	2.21	0.94
Steel B	0.111	0.31	0.40	0.025	2.25	0.90

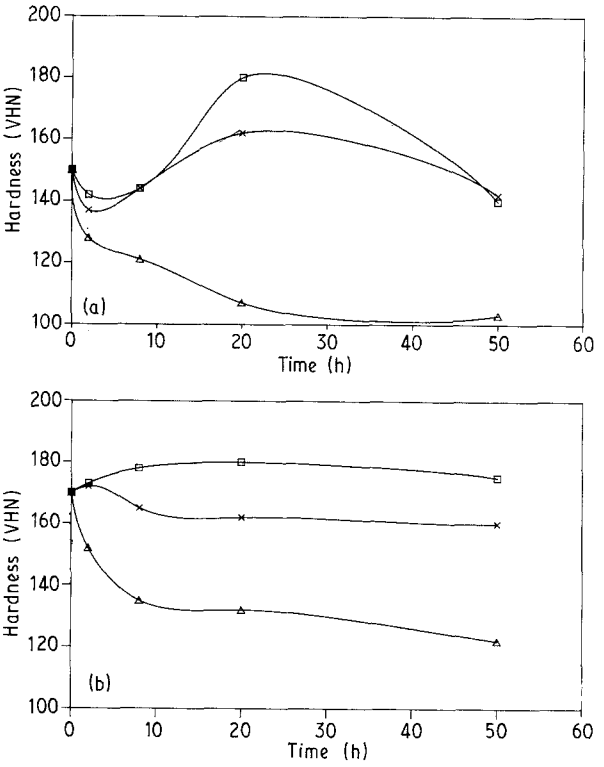

Figure 1 Variation in microhardness in (a) steel A and (b) steel B with tempering time at various temperatures. (a) ×, 823 K; □, 923 K; △, 1023 K. (b) □, 823 K; ×, 923 K; △, 1023 K.

Fig. 4a and b shows the morphology of carbides within bainite in AC condition for steels A and B, respectively. It is clear from the figures that the number density and size of carbide particles in bainite of steel B are higher than that found in steel A. The analysis of selected area diffraction (SAD) patterns taken from the carbides shown in Fig. 4a and b confirms that the precipitates are cementite particles. Fig. 4c shows the typical SAD pattern of one of the carbides, the analysis of which indicates that they are orthorhombic cementite particles. Further, the ferrite regions of steel B in AC condition exhibited needle-like precipitates (Fig. 4d) which are expected to be M_2C. The absence of acicular ferrite in the argon-cooled steels (Figs 2 and 4) confirms that the argon cooling of $2\frac{1}{4}$ Cr 1 Mo steels does not lead to the formation of classical upper or lower bainite. Based on extensive studies on the morphology of bainite, Habraken *et al.* [15] have proposed that the bainite formed during continuous cooling of Cr–Mo steels is very different from that expected during isothermal transformation and hence has been termed "non-classical bainite". The mechanism of formation of bainite, which in turn influences its morphology, depends strongly on the rate of cooling in the temperature range 1023 K to 773 K. Accordingly, the CCT diagram is divided into three regions: formation of carbide-free acicular bainite for very fast cooling rates; "granular bainite" consisting of ferrite with high dislocation density which contains martensite–austenite islands at intermediate cooling rates; a mixture of polygonal ferrite and bainite, which is sometimes referred to as "pseudo pearlite", at very slow cooling rates [16].

Careful examination of many regions of the argon-cooled steels did not reveal either high density of dislocations in ferrite or the islands of austenite–martensite regions. Instead, well developed, defect-free polygonal proeutectoid ferrite grains and bainitic ferrite with a high density of randomly distributed cementite particles are observed. This suggests that the very slow cooling rate employed in the present study corresponds to region III of the classification scheme of Habraken *et al.* [15].

Fig. 5 represents the microstructure of steel A tempered at 1023 K for various times. While Fig. 5a shows precipitation of fine carbides along the ferrite–ferrite interface at 2 h, Fig. 5b depicts the coarsening of these carbides on continued tempering up to 8 h. The inset in Fig. 5b is the selected area diffraction (SAD) pattern from the carbide particles, the analysis of which confirms that they belong to $M_{23}C_6$. Unambiguous identification of $M_{23}C_6$ and M_6C is quite difficult, since their crystal structures are identical with nearly equal unit cell dimensions. However, the isothermal diagrams for the sequence of carbide formation in $2\frac{1}{4}$ Cr 1 Mo steel available in the literature [5] suggest that the onset of formation of M_6C at 1023 K is expected only after 500 h and that only $M_{23}C_6$ and not M_6C is expected at 8 h as has been confirmed also in the present study (Fig. 5b). Prolonged tempering for times up to 50 h has resulted in the precipitation of $M_{23}C_6$ within the ferrite matrix (Fig. 5c).

Although the tempering reactions led to precipitation of secondary alloy carbides, the dissolution of bainite was not complete despite prolonged tempering. Fig. 6 shows the evidence for retention of bainite and carbide replacement reactions in steel B tempered at 923 K for 20 h (Fig. 6a) and 50 h (Fig. 6b). The inset in Fig. 6a confirms the formation of the secondary alloy carbide of the M_7C_3 type. The preferential nucleation of secondary carbides occurred along ferrite–bainite boundaries (Fig. 6b). The tempering time of 20 h for the formation of M_7C_3 at 923 K in the present study is found to be slightly less than that expected from earlier work [5]. This discrepancy could be attributed to the variation in the prior microstructures and the consequent difference in the carbon potential within bainite. The initial microstructure in the present study consisted of only 30% bainite in contrast to 100% bainite in the steels used in ref. 5. It is reasonable to expect that the lower amount of bainite would inherit the carbon content of the austenite into which the proeutectoid ferrite would have rejected the excess carbon during its formation while cooling. Although steel B of the present study and the steel used in Ref. 5 were of the same initial carbon content, the carbon potential of bainite in the present study is expected to be higher than that of the steel with 100% bainite in Ref. 5. As a consequence, precipitation of M_7C_3 is found to be faster in the present study.

The microchemical constituents of the carbides in carbon extraction replicas of tempered steel were identified using analytical transmission electron microscopy (ATEM). Fig. 7 corresponds to the energy dispersive X-ray (EDX) spectrum from steel A tempered at 923 K for a period of 50 h, which shows that the carbides are rich in iron with some solubility for chromium and very little molybdenum. This iron-rich spectrum confirms the presence of undissolved cementite particles, even after prolonged tempering at 923 K, in agreement with the existing carbide stability diagrams. However, the iron-rich M_3C precipitates do have limited solubility for other elements like chromium and molybdenum in agreement with an earlier report [17].

In addition, uniform distribution of needle-shaped precipitates is observed in the ferrite matrix. The presence of such carbides in ferrite is seen quite frequently, typical evidence for which is presented in Fig. 8. These fine, acicular carbides introduce intense streaking in the corresponding diffraction pattern, as shown in the inset of Fig. 8, the direction of streaking being parallel to $\langle 1\,1\,0\rangle_\alpha$. The streaking observed in the electron diffraction pattern can be attributed to the lattice strain introduced by the M_2C precipitates ($\simeq 30$ nm in width) in ferrite. This matrix strain has been attributed to the secondary hardening observed during tempering, which is discussed later. The axis of the elongated carbide particles, which represents the growth direction of the particles, is found to be $\langle 1\,1\,0\rangle_\alpha$ which agrees with the growth direction of M_2C in the Fe–Mo–C system reported earlier [18].

The results presented above may be summarized as follows:

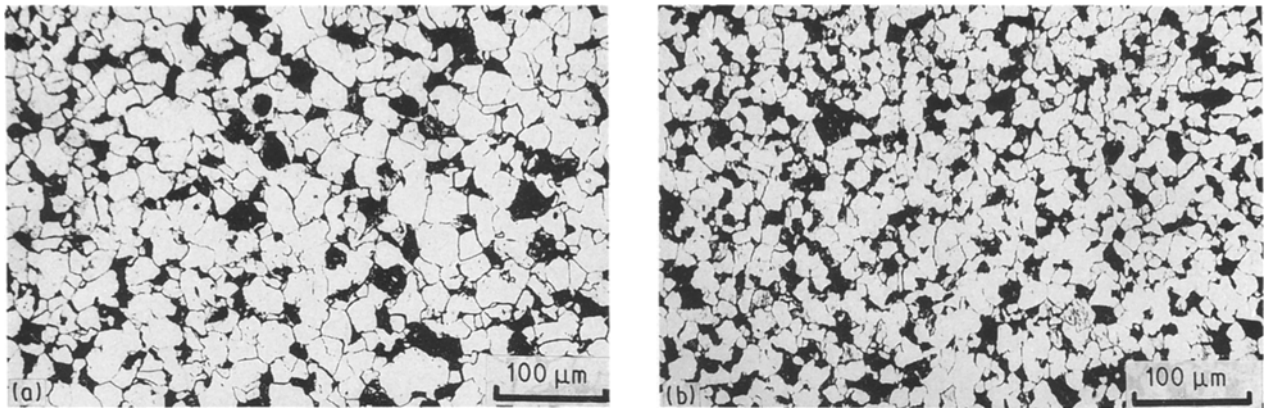

Figure 2 (a) Optical micrograph of steel A austenitized at 1323 K for 1 h followed by argon cooling (AC). (b) Optical micrograph of steel B in austenitized and argon-cooled condition.

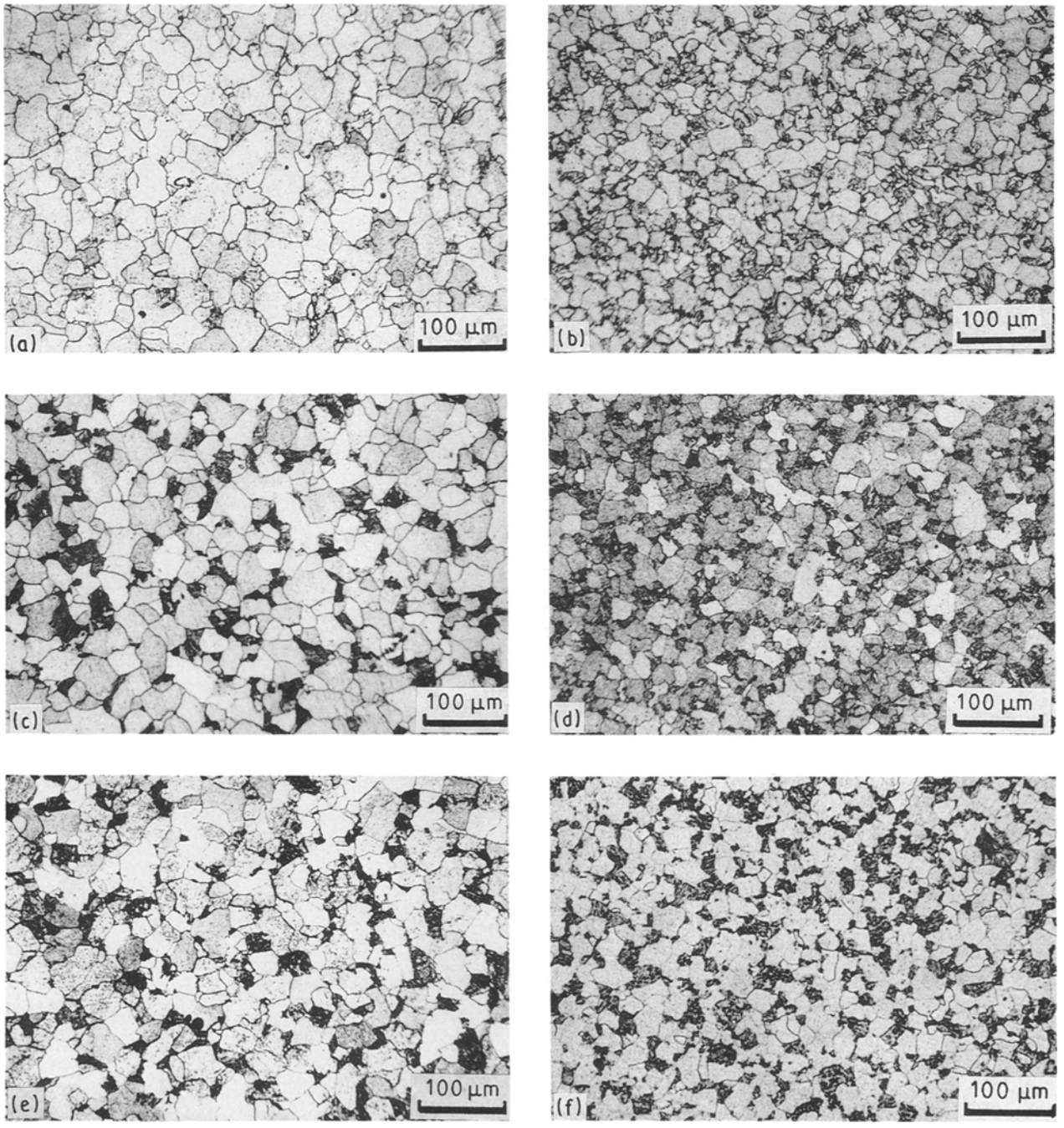

Figure 3 Optical micrographs of the two steels for various tempering treatments illustrating the difference in the dissolution rate of bainite. (a) Complete dissolution of bainite in steel A tempered at 1023 K for 2 h; (b) retention of bainite in steel B after the same treatment as in (a); (c) resistance to dissolution of bainite in steel A tempered at 923 K for 50 h; (d) steel B tempered at 923 K for 50 h; (e) steel A tempered at 823 K for 50 h; (f) steel B tempered at 823 K for 50 h.

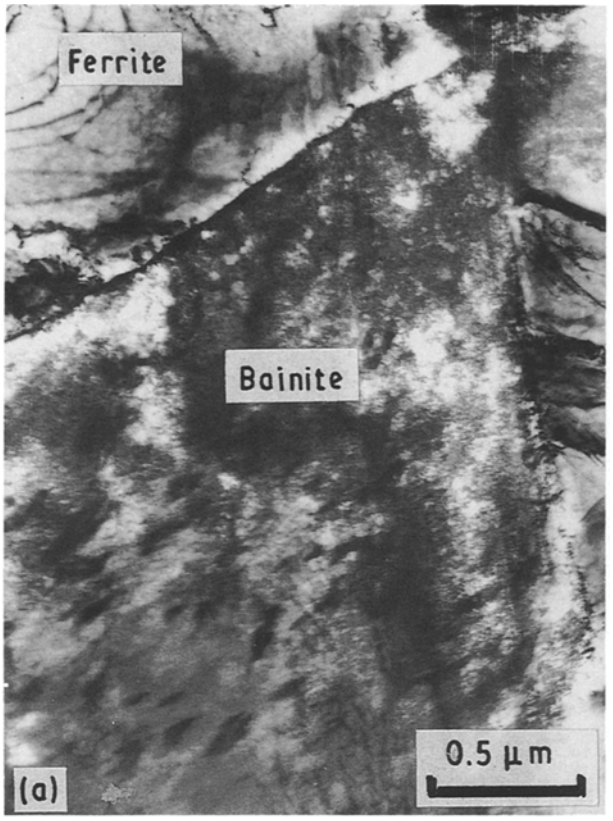

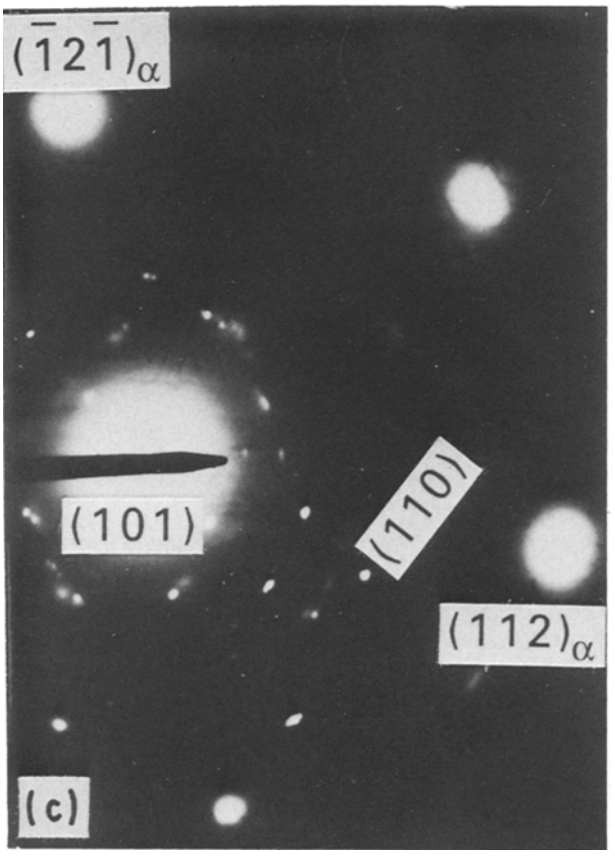

Figure 4 (a) Transmission electron micrograph showing bainite and ferrite in steel A in austenitized and argon-cooled condition; (b) transmission electron micrograph showing the presence of bainite and ferrite in steel B in austenitized and argon-cooled condition; (c) SAD pattern from the carbides shown in (b) confirming the presence of cementite with $\langle \bar{1}\,1\,1 \rangle$ zone axis; (d) transmission electron micrograph showing presence of fine needle-like precipitates in the ferrite region of steel B in argon-cooled condition.

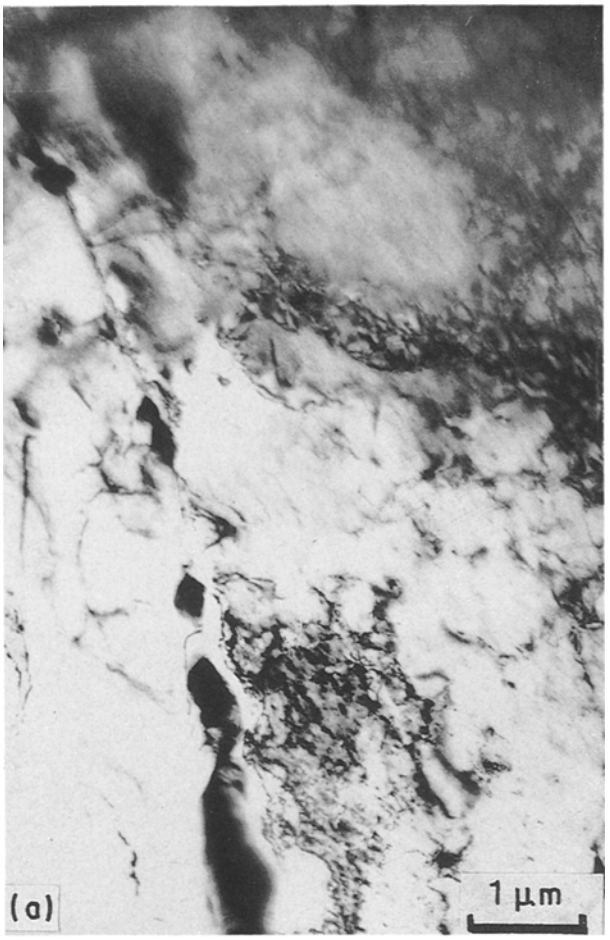

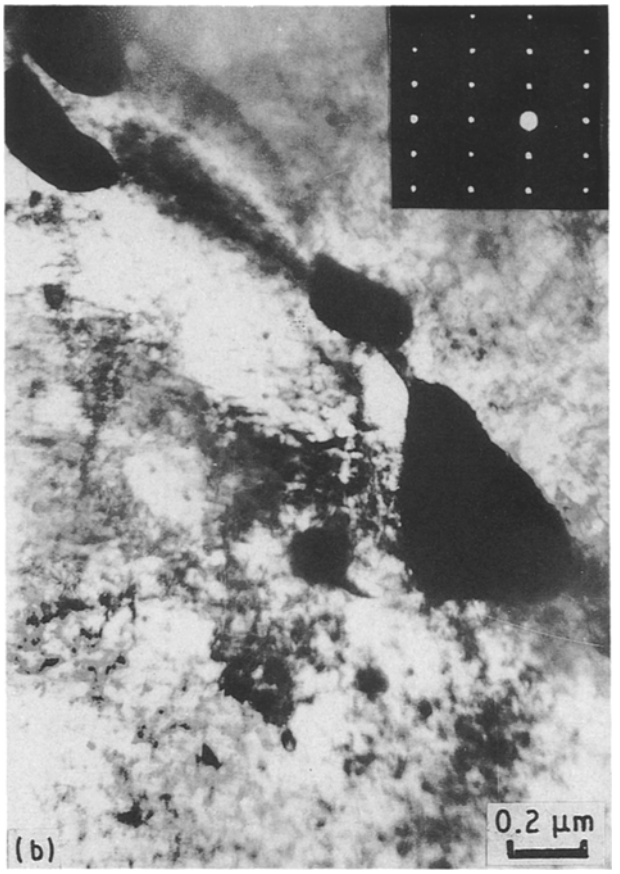

Figure 5 (a) Transmission electron micrograph of steel A tempered at 1023 K for 2 h; (b) transmission electron micrograph of steel A tempered at 1023 K for 8 h, the inset shows SAD of $M_{23}C_6$ with $\langle 2\bar{2}0 \rangle$ zone axis; (c) transmission electron micrograph of steel A tempered for 50 h at 1023 K.

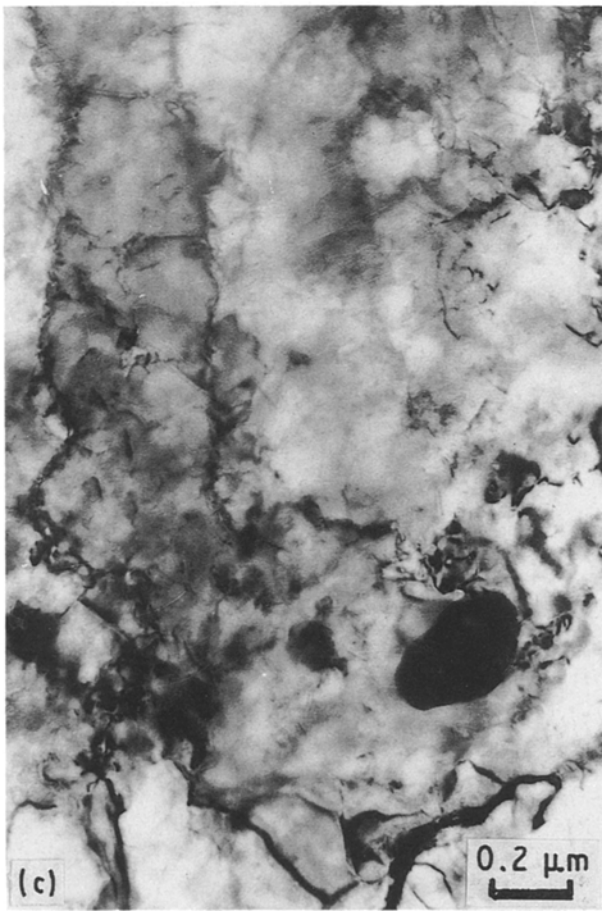

(a) The initial (AC condition) amount of bainite was more in steel B than in steel A.
(b) The dissolution rate of bainite was found to be higher in low C steel and at high tempering temperatures.
(c) During tempering, secondary carbides replaced primary cementite; coarse carbides precipitate along interfaces and acicular carbides precipitated uniformly within ferrite.
(d) EDX results suggest that the carbides Fe_3C which are rich in Fe with a little solubility for other elements are retained even after 50 h of tempering at 923 K.

4. Discussion

The general trend in the tempering behaviour of $2\frac{1}{4}$ Cr 1 Mo steel in the tempering range 823–1023 K is schematically shown in Fig. 9, which can be classified into four distinct stages. It can be seen that all four stages need not be present at all temperatures and carbon levels, the occurrence of any stage depends strongly on the predominance of the governing mechanism of each stage. Stage I is characterized by a rapid softening of the steel followed by a gradual increase in the hardness reaching a maximum in stage II. Yet another steep reduction in hardness level is observed

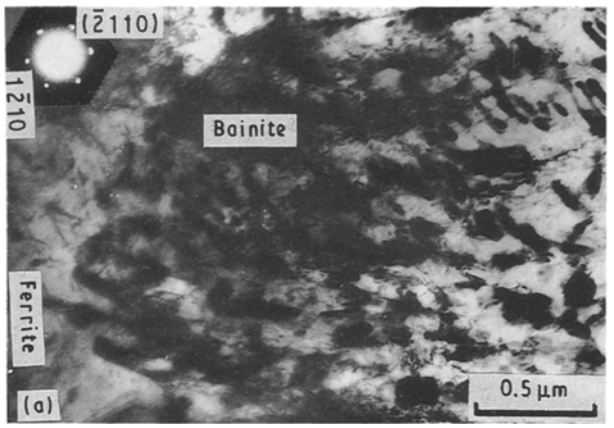

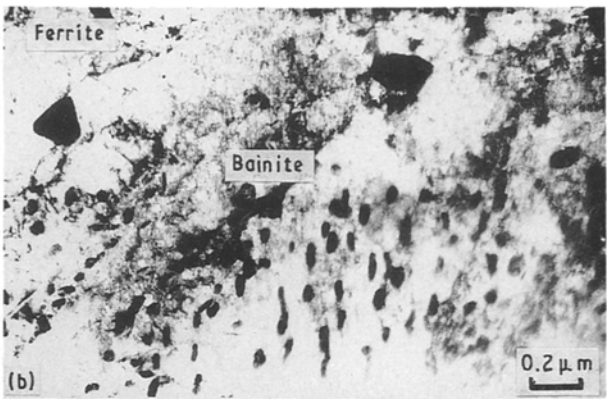

Figure 6 (a) Micrograph showing bainite and secondary alloy carbides in steel B tempered at 923 K for 20 h. Inset shows evidence of M_7C_3. (b) Transmission electron micrograph of steel B tempered at 923 K for 50 h showing retention of bainite and growth of secondary carbides along ferrite/bainite interface.

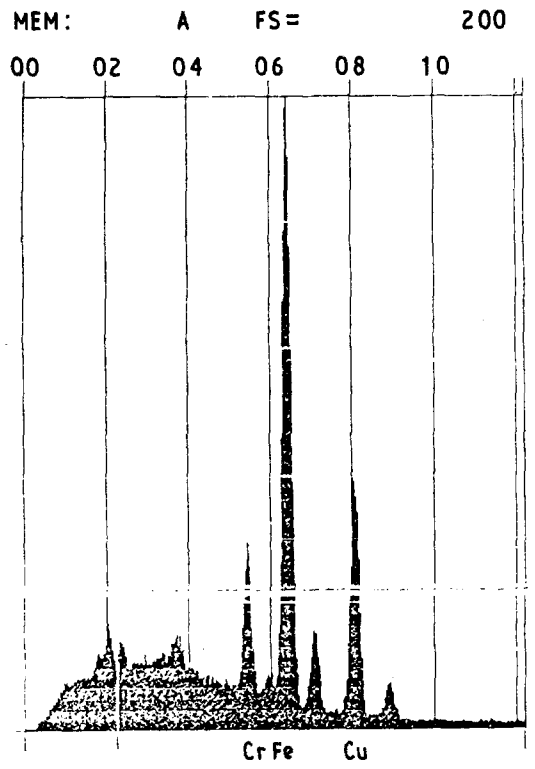

Figure 7 EDX spectrum showing the evidence for retention of bainite in steel A after tempering for 50 h at 923 K.

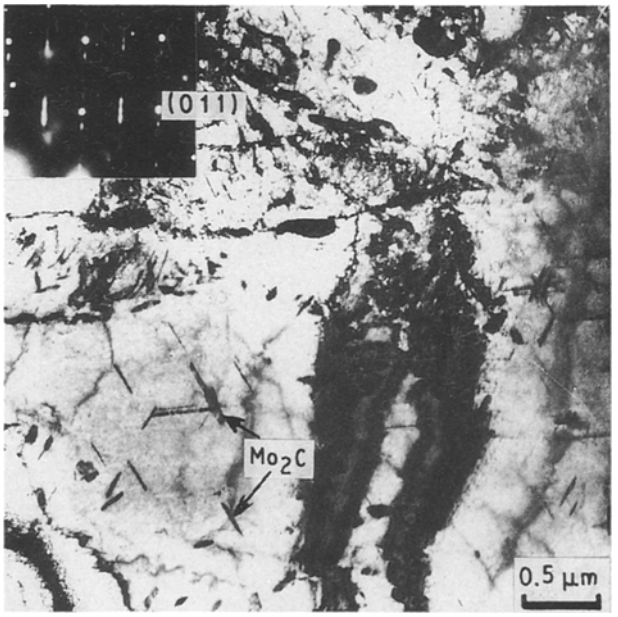

Figure 8 Micrograph showing retention of M_2C needles in steel B tempered at 923 K for 50 h. The inset shows the streaking due to the fine needles in the SAD pattern.

in stage III followed by saturation in stage IV. In the present study, stage I can be attributed to the initial rapid dissolution of cementite, prior to the onset of secondary carbide transformations. The rate of dissolution of bainite is fastest at 1023 K for both steels which, therefore, masks the influence of secondary hardening processes leading to a continuous softening at 1023 K. The highest affinity of Mo atoms for carbon atoms results in the formation of Mo–C clusters, which gradually grow and eventually transform into coherent M_2C precipitates. These precipitates introduce intense strain in the ferrite lattice leading to hardening of the steels. Stage II is a consequence of these processes. These fine precipitates, on further tempering, lose their coherency and consequently ma-

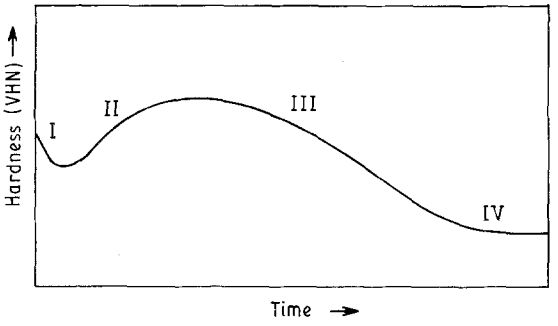

Figure 9 Schematic representation of various stages of tempering behaviour in $2\frac{1}{4}$ Cr 1 Mo steel. Stage I is the initial continuous softening due to rapid dissolution of bainite in AC steels, evidence for which is shown in Fig. 3a and b. Stage II is attributed to hardening due to precipitation of fine needle-like M_2C carbides (Figs 4d and 8). Stage III is due to precipitation of M_7C_3 etc. (Figs 5 and 6). Stage IV is caused by slow overageing kinetics of coarse carbides (Fig. 6).

trix strain is relieved resulting in further softening during stage III. The saturation after prolonged tempering is due to the slow overageing kinetics at longer tempering times. Similar stages of tempering behaviour, associated with different mechanisms depending on the steel, have been proposed for non-bainitic Fe–Mo–C and Fe–V–C steels [19].

Based on the microstructural observations illustrated in the previous section, the following features of tempering behaviour are explained below:

(a) High level of initial hardness for steel B than steel A.
(b) The occurrence of secondary hardening preferentially at lower temperatures.
(c) The presence of initial softening (stage I) prior to secondary hardening for steel A compared with its absence in steel B.
(d) The rapid tempering rate at 1023 K.
(e) The higher saturation value of hardness at 923 K and 823 K as compared with 1023 K.

The higher initial hardness exhibited by steel B in comparison with steel A in AC condition can be rationalized based on (a) the greater volume fraction of bainite (Fig. 2b), (b) higher number density of cementite particles within bainite (Fig. 4b) and (c) the presence of acicular carbides in the ferrite matrix (Fig. 4d), of steel B in the AC state.

The secondary hardening peaks observed at lower temperatures for shorter durations could be attributed to continued precipitation of needle-like M_2C carbides and their resistance to coarsening even after prolonged tempering (Fig. 8). Based on the available data on crystal lattice parameters, it is reasonable to conclude that the difference between the specific atomic volume of hcp Mo_2C (17.7×10^3 nm^3) and of the bcc ferrite (11.8×10^3 nm^3) surrounding it, is very high, leading to elastic distortion of the host lattice and the precipitate. The coherent nature of the interface between Mo_2C and ferrite (as is expected from its morphology) not only reduces the surface free energy, but also sets in coherency strain in the matrix (as confirmed by streaking in the electron diffraction pattern), which in turn is responsible for the observed secondary hardening. Similar observations of uniform dispersion of such fine acicular carbides contributing to significant strengthening in Cr–Mo steels have been reported earlier [20].

The third feature of the tempering behaviour to be understood is the presence of initial softening (at 923 K and 823 K) prior to secondary hardening in alloy A and its absence in alloy B. The difference in the carbon level is found to alter the rate of dissolution of bainite and precipitation of acicular M_2C carbides, both of which have opposing influences on the tempering behaviour. In the present study, it has been shown that the amount of bainite in the AC condition is less in steel A (Fig. 2a) than in steel B (Fig. 2b) and the rate of dissolution of bainite is higher in steel A, contributing significantly to softening. In addition, it is observed that the ferrite regions of steel A (in AC state) are completely free from M_2C carbides. These two factors, namely lower amount and faster dissolution of bainite and M_2C-free ferrite regions in the AC state, are mainly responsible for the observed softening in alloy A. Continued tempering led to the growth of M_2C carbides resulting in the observed secondary hardening in steel A. Conversely, steel B exhibited a higher amount of bainite (Fig. 2b) and high density of uniform distribution of M_2C carbides in the ferrite regions even in the AC states (Fig. 4d), leading to a high value of initial hardness level. Subsequent tempering only resulted in further nucleation and growth of M_2C carbides in ferrite leading to the observed secondary hardening. Thus, the high level of initial hardness and further growth of M_2C carbides had completely masked the initial softening prior to secondary hardening in steel B.

The absence of M_2C in ferrite regions of steel A in the AC state can be rationalized based on the smaller amount of bainite in steel A. The amount of carbon in solution in the ferrite regions is expected to be high as a consequence of the lower amount of bainite leading to a decrease in the concentration ratio of Mo:C. It is known [6] that the driving force for the precipitation of acicular M_2C carbides is considerably lowered by the reduction in the concentration ratio of Mo:C. This explains the absence of M_2C precipitates in the ferrite regions of steel A in the AC condition.

It is noticed that equilibrium $M_{23}C_6$ precipitates occur at very short tempering times (2 h, 1023 K, see Fig. 5a to c). Thus, formation of these precipitates and their coarsening cause a pronounced softening in the steels. At such high temperature, the bainite phase dissolves quite rapidly increasing the carbon activity of the ferrite matrix by the associated dissolution of the primary cementite. Under these circumstances, it is noticed that $M_{23}C_6$ carbides nucleate easily along the ferrite–ferrite interfaces and grow with time. Those carbides nucleated within the ferrite matrix coarsen much less rapidly compared with the intergranular carbides. This could be attributed to the reduction in the total free energy for the growth of such carbides since the interfaces provide part of the required surface energy. Such rapid growth of carbides leads to an early onset of overaged condition at 1023 K resulting in a pronounced softening rate during short durations of tempering. Prolonged tempering reduces the softening resulting in saturation.

The saturation value for both steels was found to be higher at 923 K and 823 K than at 1023 K. This may be understood in terms of the retention of bainite (Figs 3, 6 and 7) and resistance to coarsening of M_2C (Fig. 8) despite prolonged tempering times at these temperatures.

5. Summary

Tempering behaviour in $2\frac{1}{4}$ Cr 1 Mo steel could be classified into four stages; the specific micromechanism responsible for each stage was identified using transmission electron microscopy. Stage I, characterized by rapid softening, has been attributed to dissolution of bainite, releasing carbon into adjacent ferrite.

The relatively higher affinity of carbon for molybdenum leads to formation of Mo–C clusters which precipitate as coherent M_2C carbides resulting in secondary hardening of the steel in stage II. The loss of coherency of Mo_2C precipitates as they grow and the precipitation of secondary alloy carbides like M_7C_3, $M_{23}C_6$ etc. contribute to softening in stage III. The slow overageing kinetics of coarse carbides is responsible for saturation in hardness as in stage IV.

The variation in the kinetics of tempering behaviour with carbon content and temperature of tempering has been established and explained in terms of the differences in the rate of associated microstructural transformations.

Acknowledgements

The authors are grateful to Dr Placid Rodriguez, Head of the Materials and Metallurgy Programme, and Mr J. B. Gnanamoorthy, Head of the Metallurgy Division, for their constant encouragement and keen interest in the present study.

References

1. C. V. SUNDARAM, P. RODRIGUEZ and S. L. MANNAN, *J. Min. Met.* (Instn. of Engineers, India) **67** (1986) 1.
2. P. PATRIACA, in Proceedings of Topical Conference on Ferritic Alloys for Use in Nuclear Energy Technologies, Utah, USA, June 1983, edited by J. W. Davis and D. J. Michael (TMS, American Institute of Mining, Metallurgical and Petroleum Engineers, 1984), p. 107.
3. M. AUBERT, B. MATHIEU and P. PETRIQUIN, *ibid.*, p. 245.
4. C. WILLBY and J. WALTERS, in Proceedings of International Conference on Ferritic Steels for Fast Reactor Steam Generators, June 1977, London, edited by S. E. Pugh and E. A. Little (BNES, London, 1978) p. 40.
5. R. G. BAKER and J. NUTTING, *J. Iron Steel Inst.* **192** (1959) 304.
6. J. PILLING and N. RIDLEY, *Met. Trans.* **13A** (1982) 557.
7. R. VISWANATHAN, *Met. Technol.* **1** (1974) 284.
8. J. H. WOODHEAD and A. G. QUARRELL, *J. Iron Steel Inst.* **203** (1965) 605.
9. J. YU, *Met. Trans.* **20A** (1989) 1561.
10. J. M. LEITNAKER, R. L. KLUEH and W. R. LAING, *ibid.* **6A** (1975) 1949.
11. R. F. KNIGHT, W. R. TYSON and G. I. SPROULE, *Met. Technol.* **11** (1986) 273.
12. J. WATANABE, J. SHINDU, J. MURAKAMI, T. ADACHI, S. AJIKI and K. MIYAR, in Proceedings of the 29th Petroleum Mechanical Engineering Conference, Texas, 1974 (American Society for Mechanical Engineers, 1974).
13. B. J. CANE and J. A. WILLIAMS, *Int. Met. Rev.* **32** (1987) 241.
14. R. L. KLUEH, *J. Nucl. Mater.* **54** (1974) 41.
15. I. J. HABRAKEN, in Proceedings of Fourth International Conference on Electron Microscopy 1 (Springer Verlag, Berlin, 1960) p. 213.
16. M. G. BUSH and P. M. KELLY, *Acta. Met.* **19** (1971) 1363.
17. J. M. TITCHMARSH, Harwell Report AERE-R9661, 1979.
18. M. G. BERRY and R. W. K. HONEYCOMBE, *Met. Trans.* **1** (1970) 3279.
19. YU. I. USTINOSHCHIKOV, *Met. Sci.* **18** (1984) 337.
20. S. SAROJA, M. VIJAYALAKSHMI and V. S. RAGHUNATHAN, *J. Mat. Sci.* **27** (1992) 2389.

Received 9 May 1991
and accepted 23 January 1992